

The optics and performance of dual-focus fluorescence correlation spectroscopy

**Thomas Dertinger¹, Anastasia Loman², Benjamin Ewers³,
Claus B. Müller⁴, Benedikt Krämer³, Jörg Enderlein²**

¹UCLA, Department of Chemistry and Biochemistry, University of California, Los Angeles, CA 90095, USA

²Institute for Physical and Theoretical Chemistry, Eberhard Karls University Tübingen,

Auf der Morgenstelle 8, D-72076 Tübingen, Germany

³PicoQuant GmbH, 12961 Berlin, Germany

⁴Institute of Physical Chemistry, RWTH Aachen University, 52056 Aachen, Germany.

*Corresponding author: joerg.enderlein@uni-tuebingen.de

Abstract: Fluorescence correlation spectroscopy (FCS) is an important spectroscopic technique which can be used for measuring the diffusion and thus size of fluorescing molecules at pico- to nanomolar concentrations. Recently, we introduced an extension of conventional FCS, which is called dual-focus FCS (2fFCS) and allows absolute diffusion measurements with high precision and repeatability. It was shown experimentally that the method is robust against most optical and sample artefacts which are troubling conventional FCS measurements, and is furthermore able to yield absolute values of diffusion coefficients without referencing against known standards. However, a thorough theoretical treatment of the performance of 2fFCS is still missing. The present paper aims at filling this gap. Here, we have systematically studied the performance of 2fFCS with respect to the most important optical and photophysical factors such as cover slide thickness, refractive index of the sample, laser beam geometry, and optical saturation. We show that 2fFCS has indeed a superior performance when compared with conventional FCS, being mostly insensitive to most potential aberrations when working under optimized conditions.

©2008 Optical Society of America

OCIS codes: (170.6280) Spectroscopy, fluorescence and luminescence; (180.1790) Confocal Microscopy;(300.2530) Fluorescence, laser-induced.

References and links

1. D. Magde, E. Elson, and W. W. Webb "Thermodynamic fluctuations in a reacting system - measurement by fluorescence correlation spectroscopy," *Phys. Rev. Lett.* **29**, 705-708, (1972).
 2. E. L. Elson and D. Magde "Fluorescence Correlation Spectroscopy I. Conceptual Basis and Theory," *Biopolymers* **13**, 1-27 (1974).
 3. D. Magde, E. Elson, and W. W. Webb "Fluorescence Correlation Spectroscopy II. An Experimental Realization," *Biopolymers* **13**, 29-61 (1974).
 4. J. Widengren and Ü. Mets, *Single-Molecule Detection in Solution - Methods and Applications*, Eds. C. Zander, J. Enderlein, and R. A. Keller (Wiley-VCH, 2002) pp. 69-95.
 5. R. Rigler and E. Elson, Eds. *Fluorescence Correlation Spectroscopy* (Springer, 2001).
 6. A. Benda, M. Benes, V. Marecek, A. Lhotsky, W.T. Hermens, and M. Hof, "How To Determine Diffusion Coefficients in Planar Phospholipid Systems by Confocal Fluorescence Correlation Spectroscopy," *Langmuir* **19**, 4120-4126 (2003).
 7. J. Humpolicková, E. Gielen, A. Benda, V. Fagulova, J. Vercammen, M. VandeVen, M. Hof, M. Ameloot, and Y. Engelborghs, "Probing Diffusion Laws within Cellular Membranes by Z-Scan Fluorescence Correlation Spectroscopy," *Biophys. J. Biophys. Lett.* **91**, L23-L25 (2006).
 8. J. Ries and P. Schwille, "Studying Slow Membrane Dynamics with Continuous Wave Scanning Fluorescence Correlation Spectroscopy," *Biophys. J.* **91**, 1915-1924 (2006).

9. Z. Petrasek and P. Schwille, "Precise measurement of diffusion coefficients using scanning fluorescence correlation spectroscopy," *Biophys. J.* **94**, 1437-1448 (2008).
 10. T. Dertinger, V. Pacheco, I. von der Hocht, R. Hartmann, I. Gregor, and J. Enderlein, "Two-focus fluorescence correlation spectroscopy: A new tool for accurate and absolute diffusion measurements," *ChemPhysChem* **8**, 433-443 (2007).
 11. A. Loman, T. Dertinger, F. Koberling, and J. Enderlein, "Comparison of optical saturation effects in conventional and dual-focus fluorescence correlation spectroscopy," *Chem. Phys. Lett.* **459**, 18-21 (2008).
 12. M. Böhmer, F. Pampaloni, M. Wahl, H. J. Rahn, R. Erdmann, and J. Enderlein, "Time-resolved confocal scanning device for ultrasensitive fluorescence detection," *Rev. Sci. Instrum.* **72**, 4145-4152 (2001).
 13. B. K. Müller, E. Zaychikov, C. Bräuchle, and D. C. Lamb, "Pulsed interleaved excitation," *Biophys. J.* **89**, 3508-3522 (2005).
 14. G. Nomarski, "Interference Microscopy - State of Art and Its Future," *J. Opt. Soc. Am.* **60**, 1575-1575 (1970).
 15. E. Wolf, "Electromagnetic diffraction in optical systems I. An integral representation of the image field," *Proc. Roy. Soc. London A* **253**, 349-357 (1959).
 16. B. Richards and E. Wolf, "Electromagnetic diffraction in optical systems II. Structure of the image field in an aplanatic system," *Proc. Roy. Soc. London A* **253**, 358-379 (1959).
 17. P. R. T. Munro and P. Török, "Vectorial, high numerical aperture study of Nomarski's differential interference contrast microscope," *Opt. Express* **13**, 6833-47 (2005).
 18. P. Török, Z. Varga, G. R. Laczik, and J. Booker, "Electromagnetic diffraction of light focused through a planar interface between materials of mismatched refractive indices: an integral representation," *J. Opt. Soc. Am. A* **12**, 325 (1995).
 19. P. Török and P. Varga, "Electromagnetic diffraction of light focused through a stratified medium," *Appl. Opt.* **36**, 2305 (1997).
 20. A. Egner, M. Schrader, and S. W. Hell, "Refractive index mismatch induced intensity and phase variations in fluorescence confocal, multiphoton and 4Pi-microscopy," *Opt. Commun.* **153**, 211 (1998).
 21. O. Haeberlé, "Focusing of light through a stratified medium: a practical approach for computing microscope point spread functions. Part II: confocal and multiphoton microscopy," *Opt. Commun.* **235**, 1 (2004).
 22. O. Haeberlé, M. Ammar, H. Furukawa, K. Tenjimbayashi, and P. Török, "The point spread function of optical microscopes imaging through stratified media," *Opt. Express* **11**, 2964 (2003).
 23. I. Gregor and J. Enderlein "Focusing astigmatic Gaussian beams through optical systems with a high numerical aperture," *Opt. Lett.* **30**, 2527-9 (2005).
 24. J. Enderlein, I. Gregor, D. Patra, T. Dertinger, and U. B. Kaupp, "Performance of Fluorescence Correlation Spectroscopy for Measuring Diffusion and Concentration," *ChemPhysChem* **6**, 2324-2336 (2005).
 25. M. Leutenegger, R. Rao, R. A. Leitgeb, and T. Lasser, "Fast focus field calculations," *Opt. Express* **14**, 11277-11291 (2006).
 26. I. Gregor, D. Patra, and J. Enderlein, "Optical Saturation in Fluorescence Correlation Spectroscopy under Continuous-Wave and Pulsed Excitation," *ChemPhysChem* **6**, 164-70 (2005).
 27. P. Török, P. D. Higdon, and T. Wilson, "Theory for confocal and conventional microscopes imaging small dielectric scatterers," *J. Mod. Opt.* **45**, 1681-1698 (1998).
 28. P. D. Higdon, P. Török, and T. Wilson, "Imaging properties of high aperture multiphoton fluorescence scanning optical microscopes," *J. Microsc.* **193**, 127-141 (1999).
 29. P. Török, "Propagation of electromagnetic dipole waves through dielectric interfaces," *Opt. Lett.* **25**, 1463-1465 (2000).
 30. M. Leutenegger and T. Lasser, "Detection efficiency in total internal reflection fluorescence microscopy," *Opt. Express* **16**, 8519-8531 (2008).
 31. M. Wahl, I. Gregor, M. Paiting, and J. Enderlein, "Fast calculation of fluorescence correlation data with asynchronous time-correlated single-photon counting," *Opt. Express* **11**, 3583-91 (2003).
 32. C. B. Müller, K. Weiß, W. Richtering, A. Loman, and J. Enderlein, "Calibrating Differential Interference Contrast Microscopy with dual-focus Fluorescence Correlation Spectroscopy," *Opt. Express* **16**, 4322-9 (2008).
 33. C. B. Müller, A. Loman, V. Pacheco, F. Koberling, D. Willbold, W. Richtering, and J. Enderlein, "Precise Measurement of Diffusion by Multi-Color Dual-Focus Fluorescence Correlation Spectroscopy," *Eur. Phys. Lett.* **83**, 46001 (2008).
 34. G. Donnert, C. Eggeling, and S. W Hell, "Major signal increase in fluorescence microscopy through dark-state relaxation," *Nature Meth.* **4**, 81-86 (2007).
 35. G. Nishimura and M. Kinjo "Systematic error in fluorescence correlation measurements identified by a simple saturation model of fluorescence," *Anal. Chem.* **76**, 1963-1970 (2004).
 36. K. Berland and G. Shen, "Excitation Saturation in Two-Photon Fluorescence Correlation Spectroscopy," *Appl. Opt.* **42**, 5566-5576 (2003).

37. I. Gregor, D. Patra, and J. Enderlein, "Optical Saturation in Fluorescence Correlation Spectroscopy under Continuous-Wave and Pulsed Excitation," *ChemPhysChem* **6**, 164-170 (2005).

1. Introduction

Fluorescence correlation spectroscopy (FCS) was invented more than 30 years ago [1-3] and has seen a tremendous renaissance over the last decade due to the wide availability of affordable laser sources, low-noise single-photon detectors, and microscope objectives with nearly perfect imaging quality at high numerical apertures (N.A.). In particular, FCS has become an invaluable tool for studying the diffusion of molecules [4,5] at nanomolar concentrations, i.e. close to the infinite dilution limit. However, as pointed out in numerous publications, conventional single-focus FCS suffers from its sensitivity to a wide array of optical and photophysical factors such as laser beam quality, cover-slide thickness variation, refractive index mismatch, or optical saturation of fluorescence. The main reason for this sensitivity is the lack of an invariable length scale in the measurement: FCS probes the diffusion of molecules out of the detection volume of a confocal microscope, and any change of that detection volume will result in a change of the measured autocorrelation curve (ACF) and thus extracted value of a diffusion coefficient.

Recently, several modifications of FCS have been proposed and successfully implemented that aim at overcoming this problem. Among them are z-scan FCS [6,7], a method allowing for exact and absolute diffusion measurements in membranes, and line-scan FCS [8,9], combining spatial and temporal correlation while scanning a focus in a well-defined manner. We introduced another modification of FCS, dual-focus FCS (2fFCS), which introduces an external invariable length scale by creating two identical but laterally shifted and overlapping foci with a fixed distance between them [10]. By measuring the ACF from each focus as well as the cross-correlation function (CCF) between both foci and applying a global fit to all curves, one can extract absolute values of diffusion coefficient if the interfocal distance is well known. Ideally, many of the aforementioned experimental conditions such as laser beam quality or refractive index mismatch will change the size and shape of the detection volume of each focus but not the center distance between them. Thus, 2fFCS should in theory be largely insensitive to optical aberrations introduced by all these factors. Indeed, as was experimentally shown in Refs.[10,11], 2fFCS seems to be quite insensitive to refractive index mismatch and cover-slide thickness variation (which result in quite similar aberrations), as well as optical saturation.

The main purpose of the present paper is to present a methodical theoretical study of the performance of 2fFCS and to find optimal experimental parameters for performing 2fFCS measurements. The theoretical study allows us to systematically vary all relevant experimental parameters and to check performance of 2fFCS with respect to their variations. The paper is organized as follows: First, we briefly describe how to calculate the molecule detection functions (MDF) and thus size and shape of the detection volumes of a 2fFCS set-up, taking into account all possible aberrations. Second, we describe how to use the calculated MDF for calculating the ACFs and CCF that would be measured by a 2fFCS experiment under the given optical and photophysical conditions. Third, these calculated curves are then fitted with a standard fit routine as used for real 2fFCS measurements, and the dependence of the obtained values of the diffusion coefficient are presented as a function of different experimental conditions. A discussion of the obtained results concludes the paper.

2. Theoretical background

2.1 Calculation of the molecule detection function

A typical 2fFCS set-up is shown in Fig.1. It is based on a conventional confocal epifluorescence microscope as described in detail in Ref.[12]. However, instead of using a single

excitation laser, the light of two identical, orthogonally-polarized pulsed lasers is combined by a polarizing beam splitter. The lasers are pulsed alternately with a sufficiently high repetition rate ($\sim 10 - 80$ MHz) in so-called pulsed interleaved excitation or PIE mode [13]. Both beams are usually coupled into a polarization maintaining single mode fiber for optical cleaning. At the fiber output, the light is again collimated into a parallel light beam consisting of a train of laser pulses with alternating orthogonal polarization. The beam is then reflected by a dichroic mirror towards the microscope's objective. Before entering the objective, the light beam is passed through a Nomarski prism that is normally exploited for differential interference contrast (DIC) microscopy [14]. The principal axes of the Nomarski prism are aligned with the orthogonal polarizations of the laser pulses, so that the prism deflects the laser pulses into two different directions according to their corresponding polarization. After focusing the light through the objective, two overlapping excitation foci are generated, with a small lateral shift between them. The distance between the beams is uniquely defined by the properties of the DIC prism. Fluorescence is collected by the same objective (epi-fluorescence setup), passed through the DIC prism and the dichroic mirror, and focused into a single circular aperture which is positioned symmetrically with respect to the optical axis and chosen large enough to allow the passing of light from both detection volumes.

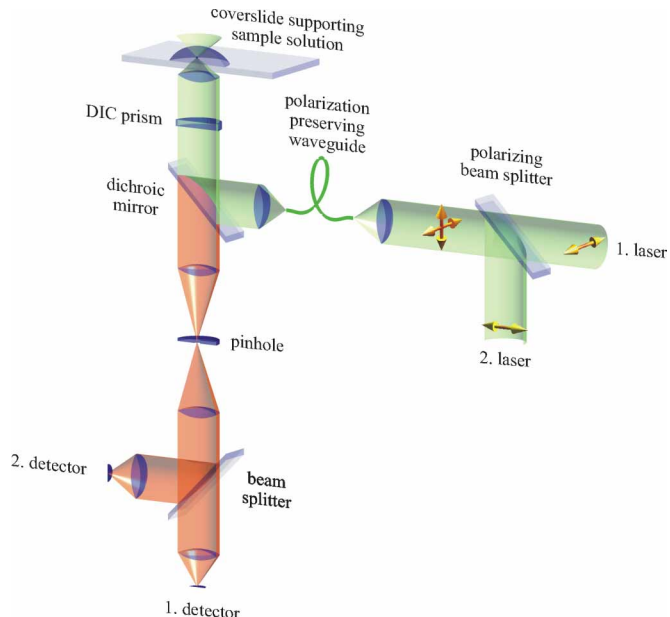


Fig. 1. Schematic of a 2fFCS set-up as theoretically studied in the present paper. For details see main text.

After the pinhole, the light is collimated, split and focused onto single-photon counting detectors. A dedicated single-photon counting device is used to record the detected photons. The nanosecond arrival times of each recorded photon are used to determine which laser has excited which fluorescence photon, i.e. in which laser focus alias detection volume the light was generated. To accomplish this unequivocally, pulse distance between laser pulses has to be sufficiently larger than the fluorescence lifetime. By knowing which photon was generated in which detection volume, autocorrelations for each detection volume as well as cross correlation functions between the two detection volumes can be calculated.

The calculation of the MDFs for both foci of the 2fFCS system as shown in Fig. 1 proceeds in two steps: (i) calculating the excitation intensity profile, and (ii) calculating the light

collection efficiency function (CEF). For rapidly rotating molecules with rotational diffusion times much faster than their fluorescence decay time, the MDF is well approximated by the simple product of the excitation light intensity distribution with the CEF, and we will limit our considerations to exactly this case. We have previously verified that taking into account slow rotational diffusion and thus fluorescence anisotropy effects has a rather negligible effect on FCS measurements [24].

In all further considerations, we make the assumption that the fluorescing molecules are electric dipole absorbers and emitters. The excitation intensity distribution $I_{ex}(\mathbf{r})$ as a function position \mathbf{r} is calculated in a standard way following the seminal works by Richards and Wolf [15,16]. The core idea is to expand the electric field in sample space into a superposition of plane waves and to find the relation between polarization and amplitude of these plane waves and the polarization and amplitude of the laser beam incident on the back focal plane of the objective. This plane wave representation is ideally suited for taking into account the influence of planar layers between the objective's front lens and the focal spot, for example cover slide glass or the layers of sample solution, or the effect of astigmatism of the exciting laser beam. The presence of the DIC prism can be handled in this approach as described in Ref.[17]. The technical details of the excitation intensity calculations have been presented in great detail in several publications and will not be repeated here [18-25].

For an ideal dipole absorber, the light absorption is proportional to the square of the scalar product between electric-field amplitude vector $I_{ex}(\mathbf{r})$ and the dipole vector \mathbf{p} of the light-absorbing molecule. However, for calculating the ACF, one needs the average excitation probability of a molecule at a given position, and this probability depends also on optical saturation. Optical saturation occurs when the excitation intensity becomes so large that the molecule spends more and more time in a non-excitatory state, so that increasing the excitation intensity does not lead to a proportional increase in emitted fluorescence intensity, see. e.g. [26]. The most common sources of optical saturation are (i) excited state saturation, i.e. the molecule is still in the excited state when the next photon arrives; (ii) triplet state saturation, i.e. the molecule undergoes intersystem-crossing from the excited to the triplet state so that it can no longer become excited until it returns back to the ground state; (iii) other photo-induced transitions into a non-fluorescing state, such as the photo-induced *cis-trans*-isomerization in cyanine dyes, or the optically induced dark states in quantum dots. In Ref.[26], we have presented an extended model of how to calculate optical saturation of a molecule taking into account ground state to excited state saturation as well as triplet state (or *cis/trans* conformation) dynamics. This model can be used to calculate the average emission rate $I_{em}(\mathbf{r})$ of a molecule as a function of its position \mathbf{r} when the excitation intensity distribution $I_{ex}(\mathbf{r})$ is known. Again, we assumed that molecular rotational diffusion is much faster than the time scale of average excitation and emission rate when calculating the relation between $I_{em}(\mathbf{r})$ and $I_{ex}(\mathbf{r})$ following Ref.[26].

Next, we need to know the light collection efficiency function (CEF) as a function of position, i.e. the probability distribution to detect light from an emitting molecule at a given position \mathbf{r} . This can be calculated by integrating the Poynting energy flux over the aperture of the confocal pinhole as induced by the emission of a molecule positioned at position \mathbf{r} . Taking again into account fast rotational diffusion, the CEF is obtained by averaging the Poynting energy flux through the confocal aperture over all possible orientations of the emitting molecule. The technical details of CEF calculations have been published several times, and the reader is referred to e.g. Ref.[24,27-30].

Finally, the MDF $U(\mathbf{r})$ is given by the product of the emission rate $I_{em}(\mathbf{r})$ (as calculated from the excitation rate $I_{ex}(\mathbf{r})$ taking into account optical saturation) times the CEF. The MDF is directly dependent on the position of the molecule in sample space, and indirectly on the excitation and emission conditions. For our numerical calculations, it is convenient to repre-

sent the MDF as a Fourier series over the angular variable ϕ (angle around the optical axis of the microscope) as

$$U(\mathbf{r}) = \sum_{m=-\infty}^{\infty} U_m(\rho, z) e^{im\phi} \quad (1)$$

where (ρ, ϕ, z) represent cylindrical coordinates with the z -axis along the optical axis [24]. Such a representation simplifies subsequent calculation of the correlation functions. For moderate displacements of the focus center from the optical axis (typically 200 nm in 2fFCS) and all the optical aberrations that will be considered in this paper, it was sufficient to consider only Fourier components up to $|m| < 10$ in Eq. (1). Any inclusion of higher Fourier components did not affect the final results.

2.2 Calculation of autocorrelation and cross-correlation function

The calculation of an ACF, $g(\tau)$, is equivalent to determining the probability of detecting a photon at time $t + \tau$ if there had been a photon detection event at time t . As has been shown in detail in Ref.[24], the ACF can be calculated from the MDF as

$$g(\tau) = \pi c \sum_{m=0}^{\infty} (1 + \delta_{m,0}) \int d\rho \int dz U_m(\rho, z) F_m(\rho, z, \tau) + \left[2\pi c \int d\rho \int dz U_0(\rho, z) + I_{bg} \right]^2 \quad (2)$$

where the function F_m is given by

$$F_m(\rho, z, \tau) = \frac{2\pi i^m \exp(-\rho^2/4D\tau)}{(4\pi D\tau)^{3/2}} \int_0^{\infty} d\rho_0 \rho_0 \int_{-\infty}^{\infty} dz_0 U_m(\rho_0, z_0) J_m\left(\frac{i\rho\rho_0}{2D\tau}\right) \exp\left[-\frac{\rho_0^2 + (z - z_0)^2}{4D\tau}\right] \quad (3)$$

and the following abbreviations have been used: D is the diffusion coefficient of the diffusing molecules, c is their concentration, $\delta_{m,n}$ is Kronecker's symbol being unity for $m = n$ and zero otherwise, and J_m denotes Bessel functions of the first kind. The integrations in the above equations have to be done numerically. Because the MDF falls off rapidly to zero when moving away from the focus centre, the integrations converge rather quickly to a final value when numerically integrating over larger and larger values of ρ and z .

The calculation of the CCF between foci, for example the probability to detect a photon at time $t + \tau$ from the second focus if there had been a photon detection event at time t from the first focus, is done totally analogously to Eqs. (2) and (3), but by calculating first the F_m using the MDF of the first focus, and evaluating then the integral in Eq. (2) by using the MDF of the second focus.

2.3 Fitting of the correlation functions and extraction of diffusion coefficients

As was shown in Ref.[10], under ideal optical conditions, the MDF of a confocal microscope can be fairly well-approximated by a combination of a Gauss-Lorentzian function with a pin-hole function as

$$U(\mathbf{r}) = \frac{\kappa(z)}{w^2(z)} \exp\left\{-\frac{2}{w^2(z)} \left[\left(x \pm \frac{\delta}{2}\right)^2 + y^2 \right]\right\} \quad (4)$$

where x and y are transversal coordinates perpendicular to the optical axis $z = 0$, δ is the lateral distance between both foci, so that one focus is shifted by $+\delta/2$ and the other by $-\delta/2$ away from the optical axis along the x -axis, and the functions $\kappa(z)$ and $w(z)$ are given by

$$w(z) = w_0 \left[1 + \left(\frac{\lambda_{ex} z}{\pi w_0^2 n} \right)^2 \right]^{1/2} \quad (5)$$

and

$$\kappa(z) = 1 - \exp\left(-\frac{2a^2}{R^2(z)}\right) \quad (6)$$

where the function $R(z)$ is defined by:

$$R(z) = R_0 \left[1 + \left(\frac{\lambda_{em} z}{\pi R_0^2 n} \right)^2 \right]^{1/2}. \quad (7)$$

Here, λ_{ex} is the excitation wavelength, λ_{em} the center emission wavelength, n is the refractive index of the immersion medium (water), a is the radius of the confocal aperture divided by magnification, and w_0 and R_0 are two (generally unknown) model parameters.

When assuming such a MDF, then the lag-time τ -dependent part of the ACFs and CCF are given by the general expression

$$g(\tau, \delta) = \frac{c}{4} \sqrt{\frac{\pi}{D\tau}} \int_{-\infty}^{\infty} dz_1 \int_{-\infty}^{\infty} dz_2 \frac{\kappa(z_1) \kappa(z_2)}{8D\tau + w^2(z_1) + w^2(z_2)}. \quad (8)$$

$$\exp\left[-\frac{(z_2 - z_1)^2}{4D\tau} - \frac{2\delta^2}{8D\tau + w^2(z_1) + w^2(z_2)}\right]$$

where the ACF is found by setting δ to zero, $g_{ACF}(\tau) = g(\tau, 0)$, and the CCF is given by $g_{CCF}(\tau) = g(\tau, \delta)$. We will use Eq. (8) for globally fitting the ACFs and CCF as calculated by Eqs. (2) and (3) using the exact MDF. For this fit, the exact ACFs and CCF are calculated on a logarithmic time scale (i.e. at logarithmically spaced τ -values, similar to real experiments where correlation functions are calculated by a multiple-tau algorithm, see e.g. Ref.[31]), and fitting is performed with a least-square method. The intrinsic fit parameters, besides constant offset and vertical scaling factor, are the diffusion coefficient D , the waist parameter w_0 , and the confocal pinhole parameter R_0 . The shear distance δ of the DIC prism is assumed to be known *a priori* and is set equal to 400 nm in the following calculations.

3. Results and discussion

3.1 Anatomy of the Molecule Detection Function

Numerical calculation of the MDF Fourier coefficients $U_m(\rho, z)$ is done on a square (ρ, z) -grid with a grid spacing of $\lambda_{ex}/30$. The grid extension is chosen large enough so that the MDFs for both foci have fallen everywhere below 10^{-3} of their maximum values. Further refinement or extension of the grid size did not change the final results. All integrations in Eqs. (2) and (3) were carried out using finite element summation.

The optical parameters in our calculations have been: numerical aperture (N.A.) of the assumed water immersion objective is 1.14, magnification in the plane of the confocal aperture is 60 \times , principal plane focal distance is 3 mm, and diameter of the confocal aperture is 200 μm . For all calculations, the focal plane is assumed to be located at 20 μm above the cover-slide surface, which means that after focusing with the objective onto the sample-side surface of the cover-slide, it is moved by 20 μm further inside the sample. Although this parameter is unimportant for perfect, aberration-free focusing and imaging conditions, this value becomes relevant when considering refractive index mismatch between sample solution and the objective's immersion medium. In a first step, we calculated the MDFs of the two overlapping foci for different diameters of the incident laser beam at the objective's back focal plane. We considered $1/e^2$ -beam-radius values of 1.25, 1.5, 2, 3 and 4 mm, thus starting with a rather large focus size and ending with a focus close to the diffraction limit (with the

objective's parameters as specified above, the radius of its back focal aperture is equal to 3.42 mm). The resulting overlapping MDFs are visualized in Fig. 2.

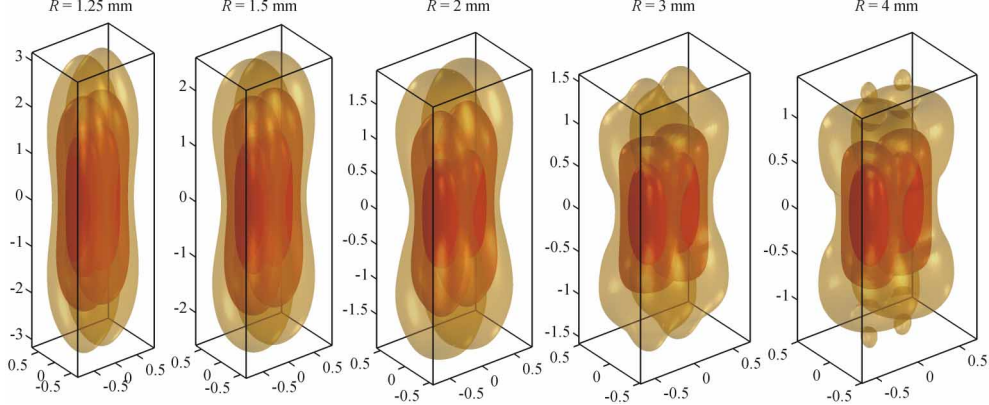


Fig. 2. Visualization of the two overlapping MDFs for different laser beam diameters as indicated above each panel. For each MDF, three iso-surfaces are shown where the MDF has fallen off to $1/e$, $1/e^2$ and $1/e^3$ of its maximum value. With increasing beam diameter, i.e. increasing laser beam focusing, the MDF becomes more structured, and for the largest beam diameter, one can clearly see the elongated shape (transverse to the optical axis) of each focus. This is typical for diffraction-limited focusing of a polarized beam by a lens with high numerical aperture.

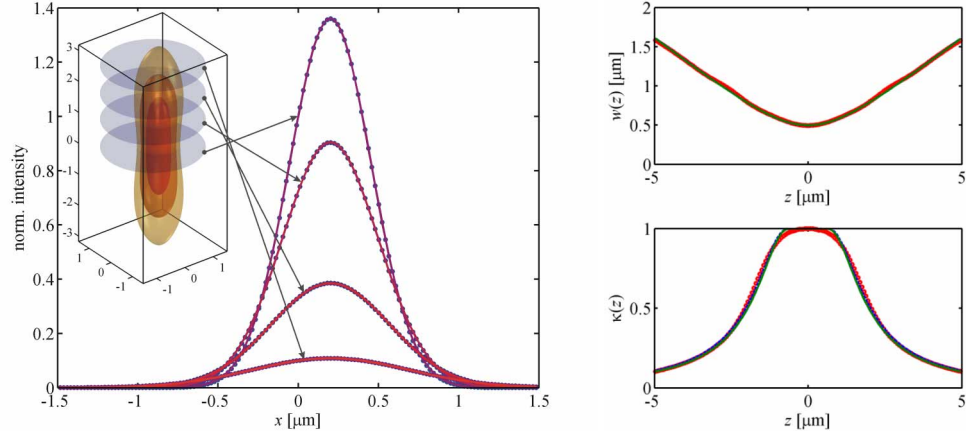


Fig. 3. (a) Left panel: Anatomy of the MDF of one of the two laser beams. Gaussian fits of the MDF distribution obtained by focusing a laser beam with radius $R = 1.25$ mm. Shown are distributions in four different cross-sections at axial positions $z = 0.0, 0.9, 1.8$, and $2.7 \mu\text{m}$. As can be seen, a Gaussian is indeed a perfect fit to the actual distribution. Right panels: Fit (blue dashed line) of the z -dependence of radius $w(z)$ and amplitude $\kappa(z)$ of the wave-optically calculated MDF (red circles) by Eqs. (5) and (6). Shown also are curves (green solid line) obtained when using the parameters w_0 and R_0 from a global fit of the ACFs and CCF using Eq. (8). The expressions of Eqs.(5) and (6) are indeed a remarkably accurate description of the actual MDF, and the correlation function fit yields parameter values quite close to the best fit of Eqs. (5) and (6) to the actual MDF.

To check the validity of the generic approximation of the MDF as presented in Eqs. (4) through (7), we fitted two-dimensional Gaussian distributions to the MDF at various cross-sections located at different positions along the optical axis, as shown in the left panels of Figs. 3(a) and (b). As can be seen, cross sections of the MDF at different positions along the optical axis can indeed be fairly well-approximated by a two-dimensional Gaussian distribu-

tion. Only when focusing close to the diffraction limit, deviations from a Gaussian profile start to show up in cross sections away from the focal plane (see left panel in Fig. 3(b)). However, the standard assumption used in conventional FCS data evaluation that the width of the Gaussian distributions does not change when moving along the optical axis is obviously far from being fulfilled. The width $w(z)$ of the Gaussian distributions as a function of the z -coordinate is shown in the top right panels of Figs. 3(a) and (b), together with a fit of Eq. (5). Furthermore, we considered the z -dependence of the MDF, i.e. $U(\rho = 0, z)$, multiplied this function by $w^2(z)$, and fitted the resulting function with the expression from Eq. (6) (bottom right panels of Figs. 3(a) and (b)). Additionally, we calculated with the MDFs the corresponding ACFs and CCF and fitted them with a global fit using Eq. (8), thus extracting values for the parameters w_0 and R_0 . We plotted in the right panels of Figs. 3(a) and (b) also the functions of Eq. (5) and Eq. (6) using these parameters as extracted from the 2fFCS fits. In the case of relaxed focusing, Fig. 4(a), the wave-optically calculated functions $w(z)$ and $\kappa(z)$ can be perfectly fitted by the model curves of Eq. (5) and Eq. (6), and moreover, these fits are in perfect agreement with the parameters w_0 and R_0 as extracted from a 2fFCS measurement fit.

The situation is different when approaching diffraction limited focusing. The Gaussian distribution looks less and less perfect when moving away from the focal plane. Also, the fit of Eqs. (5) and (6) to the actual functions as extracted from the MDF is less perfect. This becomes even worse when using Eqs. (5) and (6) with the w_0 and R_0 parameters as derived from fitting a 2fFCS measurement.

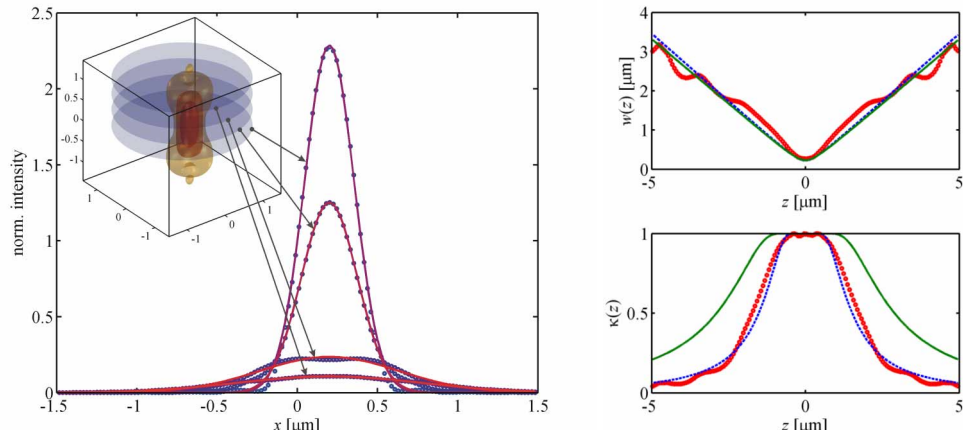


Fig. 3. (b) Same as the previous figure but for a laser beam radius of $R = 4$ mm. The chosen cross-sections are now at axial positions $z = 0.0, 0.4, 0.8$, and $1.2 \mu\text{m}$. The Gaussian approximation now shows significant deviations from the actual distributions for cross-sections farther away from the focal plane.

For the amplitude function $\kappa(z)$, the resulting curve is clearly different from the actual situation. Thus, although a 2fFCS fit yields remarkably good estimates for the structure of the MDF at relaxed focusing conditions, its description of $\kappa(z)$ gets increasingly worse when approaching diffraction-limited focusing. Thus, it is now important to ask how well a 2fFCS will estimate an absolute value of a diffusion coefficient under different focusing conditions, in particular when knowing that with coming closer to diffraction-limited focusing the extracted fit value of R_0 does not well describe the real z -dependency of $\kappa(z)$. To achieve this, we simulated 2fFCS for different focusing conditions (i.e. by changing the laser beam diameter) and fitted the resulting ACFs and CCF with Eq. (8) for extracting absolute values of the diffusion coefficient D . In the modelling we assumed that the sample molecules have some arbitrary diffusion coefficient of $5 \cdot 10^{-5} \text{ cm}^2/\text{s}$. However, this absolute values is rather unim-

portant because we will consider always the ratio between fitted and actual value of a diffusion coefficient, which will be independent on absolute values.

Figure 4 shows the ratio of fitted value of the diffusion coefficient as extracted from a 2fFCS measurement using Eq. (8) against its actual value, for different focus diameters (i.e. beam radii of incident laser beam).

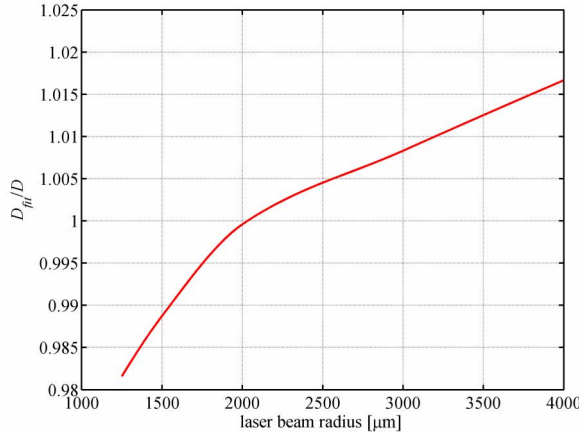


Fig. 4. Dependence of the fitted absolute value of the diffusion coefficient on laser beam diameter. Over the full range of considered radius values, the fit error is less than 2 % of its actual value. For the intermediate laser beam radius close to 2 mm, the error is negligible.

As can be seen, the relative error in absolute diffusion coefficient determination by 2fFCS is everywhere better than 2 % over the whole range of considered focusing. The increasing error with increasingly tight focusing (large laser beam radius) can be easily explained by the fact that the generic MDF model of Eqs. (4) through (7) will be an increasingly inaccurate description of the real MDF when coming closer to the diffraction limit. That we also have a systematic error at largely relaxed focusing (small laser beam radius) is due to the fact that for large focus diameters, the asymmetric clipping of the MDF by the confocal aperture, which is centred on the optical axis, becomes more and more important. The model of Eqs. (4) through (7) assumes a perfectly axisymmetric MDF for both foci, which becomes an increasingly poor assumption for larger focus diameters or when moving farther away from the focal plane. Nonetheless, even for tight focusing (laser beam radius of 4 mm), where diffraction effects already play a non-negligible role as can be seen from Fig. 4(b), the error for the extracted diffusion coefficient is still remarkably small, around 1.7 %. It should be mentioned that this is the relative error of determining the *absolute* value of the diffusion coefficient from a 2fFCS measurement, assuming that one knows the distance between foci as introduced by the DIC prism exactly (which can be measured with high precision, see Ref.[32]).

3.2 Laser astigmatism and ellipticity

Next, we studied how the accuracy of the determined value of a diffusion coefficient depends on laser beam astigmatism, that is when the beam has different focus positions within two orthogonal planes (principal planes) containing the axis of propagation [44,45]. Such astigmatism is easily introduced when using optical fibers for laser-mode cleaning, or when using (dichroic) mirrors with imperfect flat surfaces. Surprisingly, we found that laser beam astigmatism (and also laser beam ellipticity) does not have *any* effect on the accuracy of determining diffusion coefficients from 2fFCS measurements, in stark contrast to what happens for conventional single-focus FCS [24]. This is a direct consequence of the fact that with increas-

ing astigmatism, the ACF decay is shifted towards longer lag time values by the same extent as the CCF decay, so that the global fit of the 2fFCS correlation function completely cancels the effect of astigmatism.

3.3 Cover slide thickness deviation and refractive index mismatch

Two important sources of systematic errors in conventional FCS are cover-slide thickness variation (which means that the thickness of the cover-slide is different from the design value for which the objective is adjusted for) and refractive index mismatch between sample solution and the objective's immersion medium. Both effects introduce quite similar aberrations, because they are equivalent to introducing a layer of material between the objective and the focus that has a refractive index different from that of the objective's immersion medium (usually water).

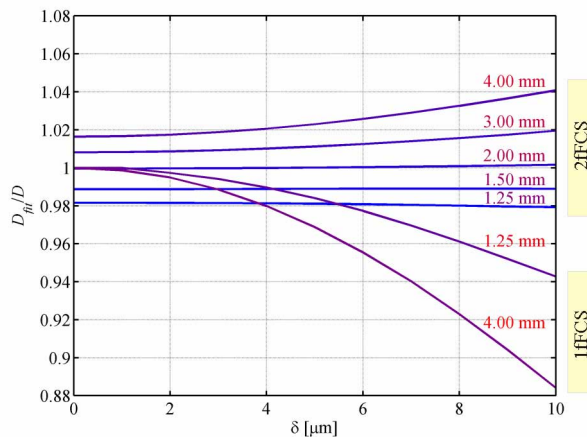


Fig. 5. Dependence of the fitted absolute value of the diffusion coefficient on cover slide thickness deviation. Shown are global fit results of a 2fFCS measurement with four different laser beam radii between 1.25 and 4 mm. For comparison, the fit results from a single-focus FCS measurement are also shown, for the two limiting laser beam radii of 1.25 and 4 mm. Because a single-focus FCS measurement cannot measure absolute diffusion coefficients, the two curves are normalized by their value at $\delta = 0 \mu\text{m}$. Remarkably, for a laser beam radius below 2 mm, a 2fFCS measurement is nearly independent on aberrations introduced by cover slide thickness deviations (and similarly, to aberrations due to refractive index mismatch).

We checked the accuracy of 2fFCS against this kind of aberration by varying the cover-slide thickness from its design value to a ten micrometer larger value (or smaller – both deviations have the same effect). In Fig. 6, we show a comparison between diffusion coefficient values as obtained from 2fFCS and from conventional FCS. It should be mentioned that conventional FCS does *not* yield *absolute* values of diffusion coefficients but must always be referenced against a sample of known diffusion – in Fig. 5, we have taken the FCS value at zero thickness deviation as the reference for all the shown single-focus FCS values. As shown, conventional FCS is much more sensitive to this kind of aberration than 2fFCS. Remarkably, there is nearly no dependence of the determined 2fFCS value on cover-slide thickness (or, similarly, refractive index mismatch) when using a laser beam radius below ~ 2 mm. This is in perfect accordance with experimental results as reported in Ref.[10,11].

3.4 Optical Saturation

The most important and most disturbing source for inaccuracy and irreproducibility in conventional FCS measurements is the dependence of the ACF decay alias diffusion time on the excitation intensity due to optical saturation of fluorescence. Ideally, the diffusion related

part of an ACF should be totally independent on excitation intensity, because it probes only the time a molecule needs to diffuse out of the detection volume, which in turn only depends on the shape and size of that volume but not on the absolute fluorescence intensity. Unfortunately, the shape and size of this volume is itself dependent upon the excitation intensity due to the non-linear relationship between excitation and fluorescence emission: with increasing excitation intensity, the fluorescence emission intensity of a molecule falls more and more behind the value that would be expected in the case of a linear dependence between excitation and emission intensity. This flattens the spatial fluorescence emission profile with respect to the excitation intensity profile and leads to an apparently larger detection volume and hence larger diffusion time.

We start by considering optical saturation connected with the $S_0 \rightarrow S_1$ transition and the finite lifetime of the excited state. We explore the saturation behaviour for a measurement with pulsed excitation using a pulse width of $0.025 \tau_f$ and repetition period of $12.5 \tau_f$ in units of the excited state lifetime τ_f .

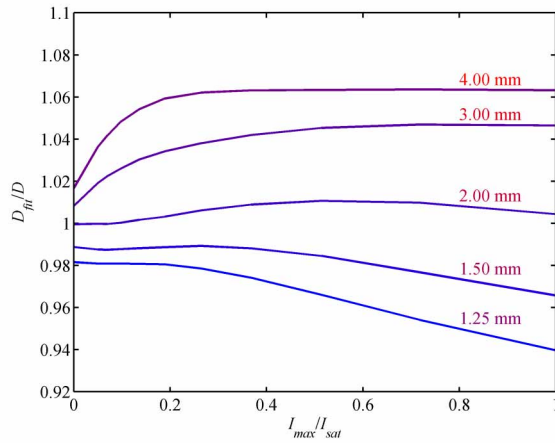


Fig. 6. Dependence of the fitted absolute value of the diffusion coefficient on excited state saturation with no intersystem crossing. Shown are the global fit results of a 2fFCS measurement with four different laser beam radii between 1.25 and 4 mm. Similar to cover-slide thickness deviation, the best results are achieved for an intermediate laser beam radius of 2 mm. In that case, the fitted value of the diffusion coefficient stays close to its actual value by better than 1 % even at high optical saturation values.

The relevant parameter determining the degree of optical saturation is the ratio of average excitation rate to saturation intensity $I_{\text{sat}} = (\sigma \cdot \tau_f)^{-1}$ (given here in units of photons per area per time), where σ denotes the molecules' absorption cross section at the excitation wavelength, see Ref.[26]. We considered saturation factors between zero and one, which means that the maximum excitation rate in the very centre of each focus was between zero and one I_{sat} . The impact of varying saturation level on the apparent diffusion coefficient D_{fit} as fitted from a corresponding 2fFCS measurement is shown in Fig. 7. There, we compare the sensitivity of 2fFCS against $S_0 \rightarrow S_1$ optical saturation for different degrees of focusing. As can be seen, for rather relaxed focusing (laser beam radius below ~ 2 mm), the method is rather insensitive to saturation as long as the maximum excitation intensity remains below $\sim 0.2 I_{\text{sat}}$. But even for rather extreme saturation values, the relative error is not larger than 7 %, again in stark contrast to conventional single-focus FCS as was analyzed in Ref.[24] and will also be shown below.

It is instructive to check in more detail how the optical saturation affects the shape and size of the MDF. In Fig. 7(a) we show how much the MDF is deformed at the extreme satura-

tion level of one, i.e. when the maximum excitation intensity in each focus is equal to I_{sat} . The considered laser beam radius was 2 mm, i.e. rather relaxed focusing.

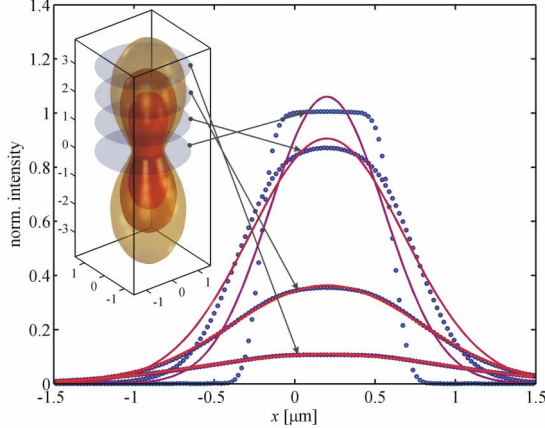


Fig. 7. (a) Anatomy of the MDF for focusing a laser beam with radius $R = 2$ mm and a $S_0 \rightarrow S_1$ optical saturation parameter of one. Clearly, the Gaussian approximation is no longer a valid approximation of the actual MDF. Remarkably, the empirical model of Eqs.(4) through (7) which lies behind the fitting of the 2fFCS measurements still yields satisfactorily accurate diffusion coefficients.

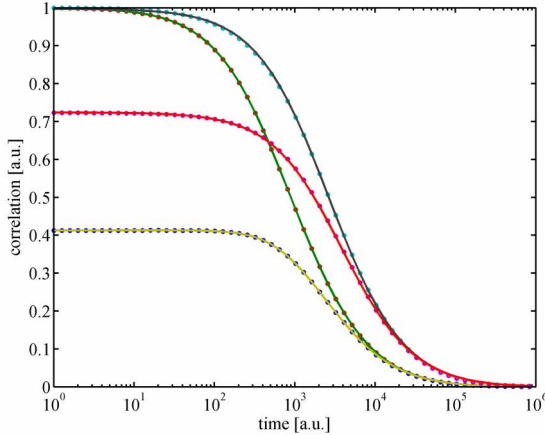


Fig. 7. (b) Fit quality of the global fit of an 2fFCS experiment under ideal optical conditions (left couple of curves) and for a $S_0 \rightarrow S_1$ optical saturation of one (right couple of curves). Dots are the theoretically calculated auto- and cross-correlation curves (cross-correlation always having lower amplitude than autocorrelation); solid lines are the best global fit. As can be seen, even under high optical saturation, apparent fit quality is still excellent.

As can be seen, the generic modified Gauss-Lorentz model for the MDF is now a rather poor representation of its real shape, but the resulting ACF and CCF curves can still be fitted extremely well with the model Eq. (8) (see Fig. 7(b)) and the extracted diffusion coefficient, as was demonstrated in Fig. 6, deviates by less than 1 % from its actual value. The reason for the relative insensitivity of 2fFCS against $S_0 \rightarrow S_1$ saturation is that, although the MDF can be heavily deformed by it, it does *not* change the distance between the foci centres. Thus again, a global fit of ACF and CCF can mostly compensate for the effects introduced by saturation. However, besides the omnipresent $S_0 \rightarrow S_1$ saturation of fluorescence, many molecules also exhibit more complex mechanisms of saturation, for example by being pumped into a non-

fluorescent triplet state or into some other non-fluorescent conformation. In this instance, it may be expected that saturation has a much stronger impact also on 2fFCS.

In the current versions of 2fFCS using PIE, the excitation between foci is switched with a high repetition rate much faster than typical triplet state transition and relaxation rates, so that the slow photophysical dynamics “sees” only an average excitation which is the sum of the excitation intensity distributions in each focus. Thus, in the region between foci the excitation intensities sum up leading to an apparent pushing-away of the centres of the two MDFs, making their effective distance larger than as assumed from the properties of the DIC prism.

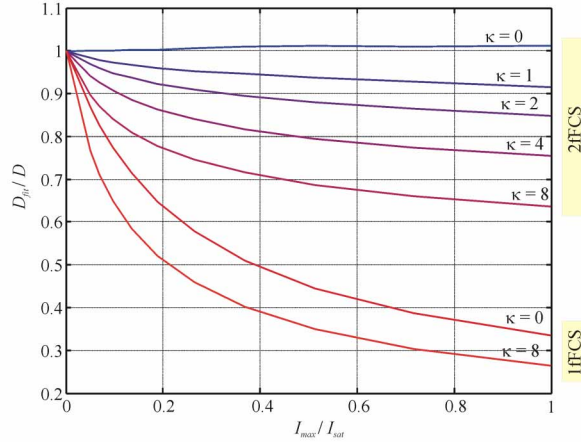


Fig. 8. Dependence of the fitted absolute value of the diffusion coefficient on excited state saturation with different ratios κ of intersystem crossing rate constant to phosphorescence rate constant, i.e. k_{isc}/k_{ph} . Shown are the global fit results of a 2fFCS measurement assuming a laser beam radius of 2 mm. For comparison, fit results from a single-focus FCS measurement are also shown, for the two limiting κ -values of 0 (no triplet state dynamics, compare with Fig.7) and 8. Because a single-focus FCS measurement cannot measure absolute diffusion coefficients, the two curves are again normalized by their value at zero optical saturation, i.e. in the limit of zero excitation intensity.

As an example, we studied the impact of triplet state pumping and relaxation. The relevant parameter describing this process is the ratio between intersystem-crossing rate constant k_{isc} and triplet-state-relaxation rate constant k_{ph} , i.e. $\kappa = k_{isc}/k_{ph}$. Figure 8 shows a comparison of the performance of conventional FCS and 2fFCS as a function of excitation intensity in units of I_{sat} for different values of κ and an assumed laser beam radius of 2 mm. As can be seen now, with increasing triplet state pumping efficiency, the outcome of a 2fFCS measurement for the diffusion coefficient becomes more and more biased towards smaller values, although the sensitivity is still not as large as in the case of conventional FCS. Interestingly, we did not find this effect in measurements on Cy5, where one has optical saturation due to a very similar optically driven process of *cis-trans* isomerization, see e.g. Ref.[11], which may be due to the fact that this transition is accelerated by light in both directions. We also checked other dyes such as Rhodamine 6G and Oregon Green [33], and again did not find a dependence of the measured diffusion coefficient on excitation intensity within a sufficiently low excitation intensity range. Nevertheless, the result shown in Fig.8 makes clear that as soon as triplet state pumping or similar light-driven photophysics takes place, it is always advisable to check the dependence of the determined diffusion coefficient on excitation intensity when using 2fFCS as well as conventional 1fFCS.

The main reason why 2fFCS is sensitive to this kind of optical saturation, as was already explained above, is that the apparent distance between the detection volumes, i.e. the lateral

distance between the maxima of the two MDFs, is getting larger with increasing saturation, as soon as the photophysical processes behind the saturation are much slower than the time between alternate pulsing in the PIE excitation scheme. However, this can also be used for circumventing this problem: Similar to the D- or T-Rex concept proposed in Ref.[34] for minimizing triplet-state (or generally dark state) related photobleaching, alternate pulsing with long intermediate waiting times that are much longer than the triplet state relaxation time will not lead to an apparent pushing away of the centres of the two overlapping MDFs and will finally lead to a similar minor dependence of the diffusion-coefficient determination accuracy on excitation intensity as was seen for the pure $S_0 \rightarrow S_1$ saturation. Thus, 2fFCS behaviour will then again be similar the curve for $\kappa = 0$ in Fig. 8 or the curves in Fig. 6, whereas the strong dependence of conventional FCS on excitation intensity still remains (see the curve for single-focus FCS with $\kappa = 0$ in Fig. 8), which has been extensively studied experimentally, see Ref.[11, 35-37].

3.5 Detection volume

Finally, let us briefly consider how precisely 2fFCS can be used for obtaining values of concentration of diffusing molecules. As is well known, the ratio of the infinite lag-time value of an ACF to its limiting value at zero lag-time (assuming no background and no fast photophysics-related decay of the ACF) is proportional to the average number of molecules within the effective detection volume V_{eff} which is defined via the MDF $U(\mathbf{r})$ as

$$V_{\text{eff}} = \left[\int d\mathbf{r} U(\mathbf{r}) \right]^2 / \int d\mathbf{r} U^2(\mathbf{r}). \quad (9)$$

The common problem in conventional FCS is that one usually does not know the exact value of V_{eff} except by calibrating it, accounting for all of the previously mentioned optical and photophysical problems that also trouble FCS as a method for precise diffusion measurements.

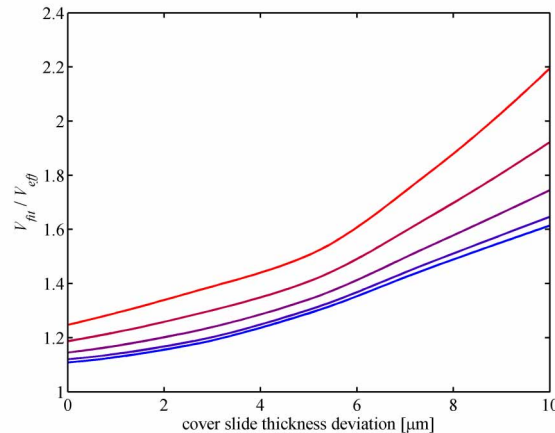


Fig. 9. Dependence of the detection volume as calculated from the empirical parameters w_0 and R_0 (as returned by the global 2fFCS fit) on cover slide thickness deviation for the four laser beam radii of 1.25, 1.5, 2, 3, and 4 mm (from bottom to top).

2fFCS also has the ability to deliver, in addition to the diffusion coefficient D , values for the MDF parameters w_0 and R_0 , which then could be used to directly calculate V_{eff} using Eq. (4) in Eq. (9). As an example demonstrating how accurate this would be, we compared the real value of V_{eff} (calculated directly from the exactly known MDF) with that which one obtains by using the model MDF Eq. (4) and the parameters w_0 and R_0 as extracted from fitting the corresponding 2fFCS curves. The result, calculated for different focusing conditions and different cover-slide thickness deviations (as a typical source of aberration), is shown in Fig. 9.

As can be seen, the performance of 2fFCS in determining absolute concentrations of molecule is much worse than its ability to yield correct values of diffusion coefficients. The reason is that the temporal decay of the ACF/CCF is obviously much less sensitive to the details of the outbound regions of the MDF, whereas the detection volume is still quite sensitive to the details of the MDF even at positions rather far away from the focal plane or the optical axis.

4. Conclusion

We have presented a thorough theoretical analysis of the performance of the recently developed 2fFCS in determining absolute values of diffusion coefficients under various optical and photophysical conditions. As was shown, under optimal excitation conditions (not too close to the diffraction limit), 2fFCS is amazingly robust against most potential sources of artefacts in conventional FCS, namely laser beam astigmatism, cover-slide thickness variation (and thus, similarly, refractive index mismatch), and, most importantly, ground-state-to-excited-state optical saturation. For triplet-state related or photophysically similar saturation processes, 2fFCS also yields a systematic error in diffusion coefficient values with increasing excitation intensity, which can, however, be easily circumvented by using more sophisticated excitation schemes with long intermediate waiting time between excitation switches from one to the other focus. Our analysis shows that 2fFCS is much superior to conventional FCS in determining precise and absolute diffusion coefficients, which will make it a useful tool wherever one needs to determine hydrodynamic radii of molecules at pico- to nanomolar concentrations.

Acknowledgment

We thank Tyler Arbour for his linguistic support and many helpful hints. Financial support by the Deutsche Volkswagenstiftung and by the Human Frontier Science Program (RGP0046/2006-C) is gratefully acknowledged.